Evolution of Enzymatic Activities in the Orotidine 5′-Monophosphate Decarboxylase Suprafamily: Crystallographic Evidence for a Proton Relay System in the Active Site of 3-Keto-L-gulonate 6-Phosphate Decarboxylase[†,‡]

Eric L. Wise,[§] Wen Shan Yew,[||] John A. Gerlt,*[,||] and Ivan Rayment*[,§]

Department of Biochemistry, University of Wisconsin, Madison, Wisconsin 53706, and Departments of Biochemistry and Chemistry, University of Illinois, Urbana, Illinois 61801

Received February 4, 2004; Revised Manuscript Received March 18, 2004

ABSTRACT: 3-Keto-L-gulonate 6-phosphate decarboxylase (KGPDC), a member of the orotidine monophosphate decarboxylase (OMPDC) suprafamily, catalyzes the Mg^{2+}-dependent decarboxylation of 3-keto-L-gulonate 6-phosphate to L-xylulose 5-phosphate. Structural and biochemical evidence suggests that the KGPDC reaction proceeds via a Mg^{2+}-stabilized 1,2-*cis*-enediolate intermediate. Protonation of the enediolate intermediate occurs in a nonstereospecific manner to form L-xylulose 5-phosphate. Although the exact mechanism of proton delivery is not known, Glu112, His136, and Arg139 have been implicated in this process [Yew, W. S., Wise, E., Rayment, I., and Gerlt, J. A. (2004) *Biochemistry 43*, 6427−6437]. Surprisingly, single amino acid substitutions of these positions do not substantially reduce catalytic activity but rather alter the stereochemical course of the reaction. Here, we report the X-ray crystal structures of four mutants, K64A, H136A, E112Q, and E112Q/H136A, each determined in the presence of L-threonohydroxamate 4-phosphate, an analogue of the enediolate intermediate, to 1.7, 1.9, 1.8, and 1.9 Å resolution, respectively. These structures reveal that substitutions of Lys64, Glu112, and His136 cause changes in the positions of the intermediate analogue and two active site water molecules that were previously identified as possible proton donors. These changes correlate with the observed alterations in the reaction stereochemistry for these mutants, thereby supporting a reaction mechanism in which water molecules competitively shuttle protons from the side chains of His136 and Arg139 to alternate faces of the *cis*-enediolate intermediate. These studies further underscore the wide variation in the reaction mechanisms in the OMPDC suprafamily.

3-Keto-L-gulonate 6-phosphate decarboxylase (KGPDC)[1] and orotidine monophosphate decarboxylase (OMPDC) are homologous enzymes that catalyze unrelated reactions which share neither a common reaction mechanism nor a common substrate specificity (*1*−*3*). KGPDC catalyzes the metal ion-dependent decarboxylation of 3-keto-L-gulonate 6-phosphate to produce L-xylulose 5-phosphate via an enediolate anion intermediate (Scheme 1) (*4*). OMPDC catalyzes the metal ion-independent decarboxylation of orotidine 5′-monophosphate to uridine 5′-monophosphate (*5*). Because of the differences in substrate identity and mechanism, KGPDC and OMPDC are said to be members of the OMPDC *supra*family (*2*).

The X-ray structures of KGPDC from *Escherichia coli* and OMPDC from several sources have been reported recently (*3*, *6*−*9*). Although their primary amino acid sequences are only 20% identical, KGPDC (Figure 1A) and OMPDC (Figure 1B) share a similar $(\beta/\alpha)_8$-fold, a nearly identical quaternary structure, and a conserved active site architecture that is constructed from conserved residues (*3*). Although the mechanism of the OMPDC reaction is still subject to discussion, it does not require a metal ion and in one scenario is thought to proceed without the formation of an energetically unfavorable vinyl anion intermediate, possibly through a concerted S_E2 electrophilic substitution mechanism. In contrast, KGPDC requires Mg^{2+} for catalytic activity, and the reaction proceeds via a 1,2-enediolate intermediate (*10*). Both enzymes share several conserved active site residues, including an aspartate at the end of the first β-strand, a lysine or glutamate at the end of the second β-strand, and a conserved Asp-x-Lys-x-x-Asp motif at the

[†] This research was supported by Grants GM-52594 (to J.A.G. and I.R.) and GM-65155 (to J.A.G. and I.R.) from the National Institutes of Health. E.L.W. was supported by the NIH Biophysics Training Grant GM08293. Use of the Argonne National Laboratory Structural Biology Center beamline at the Advanced Photon Source was supported by the U.S. Department of Energy, Office of Energy Research, under Contract W-31-109-ENG-38.

[‡] The X-ray coordinates and structure factors for the K64A, H136A, E112Q, and E112Q/H136A mutant proteins of KDPDC complexed with L-threonohydroxamate 4-phosphate have been deposited in the Protein Data Bank as entries 1SO4, 1SO3, 1SO5, and 1SO6, respectively.

* To whom correspondence should be addressed. I.R.: Department of Biochemistry, 433 Babcock Dr., Madison, WI 53706; phone, (608) 262-0437; fax, (608) 262-1319; e-mail, Ivan_Rayment@biochem.wisc.edu. J.A.G.: Department of Biochemistry, University of Illinois, 600 S. Mathews Ave., Urbana, IL 61801; phone, (217) 244-7414; fax, (217) 244-6538; e-mail, j-gerlt@uiuc.edu.

[§] University of Wisconsin.

[||] University of Illinois.

[1] Abbreviations: APS, Advanced Photon Source; KGPDC, 3-keto-L-gulonate 6-phosphate decarboxylase; OMP, orotidine 5′-monophosphate; UMP, uridine 5′-monophosphate; OMPDC, orotidine 5′-monophosphate decarboxylase; rms, root-mean-square; MePEG, methyl ether polyethylene glycol; L-THP, L-threonohydroxamate 4-phosphate.

10.1021/bi0497392 CCC: $27.50
Published on Web 05/08/2004

Scheme 1 Reactions Catalyzed by KGPDC and OMPDC

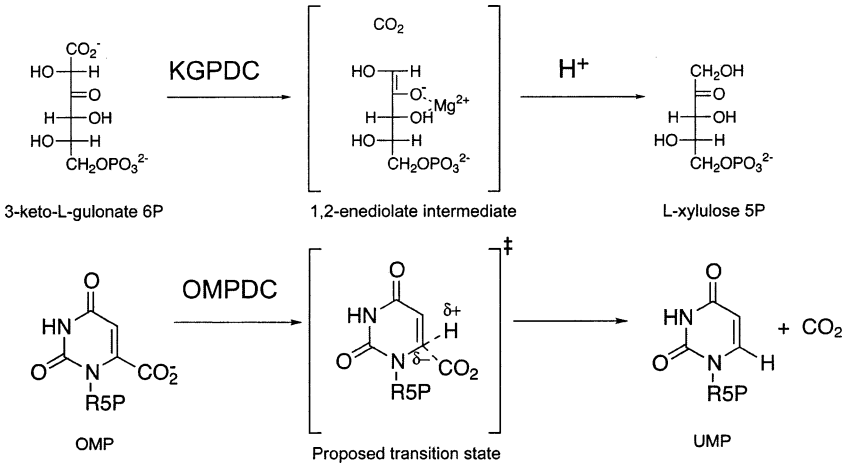

end of the third β-strand (Asp62, Lys64, and Asp67 in OMPDC from *Bacillus subtilis*). In OMPDC, the first aspartate in this Asp-x-Lys-x-x-Asp motif has been proposed to assume a critical role in the reaction by inducing ground-state destabilization of the OMP•enzyme complex through repulsive interactions with the carboxylate leaving group of OMP (*8*). The amino group of the Lys64 side chain has been proposed to act as the catalytic acid that transfers a proton to C5 of OMP. The side chain of Asp67 of the symmetry-related polypeptide in the dimer, though not directly involved in catalysis, forms a critical interaction with the ribose ring of OMP and constitutes part of an essential network of hydrogen bonds that offsets the energetically unfavorable interactions created upon substrate binding (*9*). In contrast, in KGPDC, the first aspartate in the Asp-x-Lys-x-x-Asp motif (Asp62) acts as a ligand for the Mg^{2+} ion in the active site that stabilizes the enediolate intermediate through interactions with the negatively charged oxygen on C2. The side chains of Lys64 and Asp67 interact with the oxygen atoms on C1 and C2 of the intermediate and likely function to stabilize and position the intermediate in the active site.

The identity of the general acid that delivers a proton to the enediolate intermediate in the KGPDC-catalyzed reaction is not clear. Structural and biochemical evidence suggests a role for His136 in this process (*10*, *11*). In the previously reported crystal structure of KGPDC with L-threonohydroxamate 4-phosphate (L-THP) (Figure 2A), an analogue of the *cis*-enediolate intermediate, bound in the active site, the side chain of His136 is positioned within 2.5 Å of the *si*-face of N1 of the hydroxamate group (Figure 2B) (*10*). In this location, it could function as the general acid that transfers a solvent-derived proton to the *pro-S* position of C1 of the L-xylulose 5-phosphate product. In addition, while wild-type

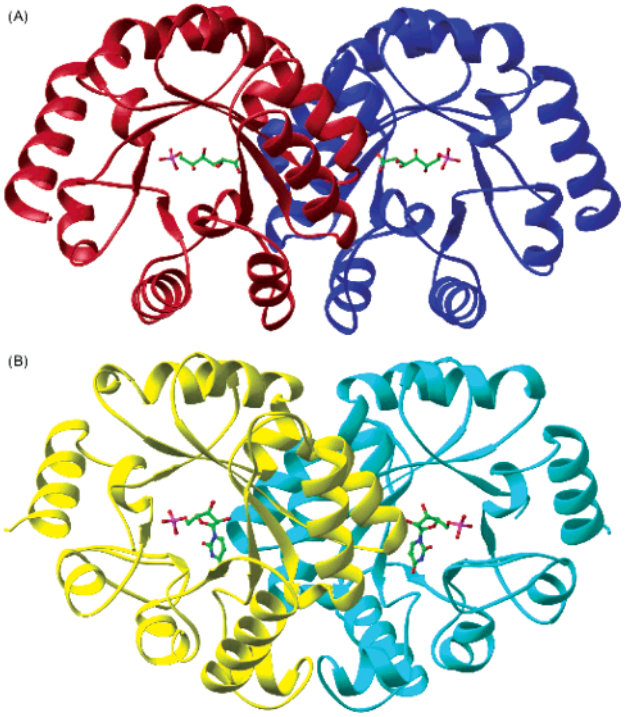

FIGURE 1: Structures of (A) KGPDC with bound L-gulonate 6-phosphate and (B) OMPDC with bound UMP. Both enzymes adopt similar $(\beta/\alpha)_8$-barrel folds and adopt similar tertiary structures. This figure was created with Ribbons (*22*).

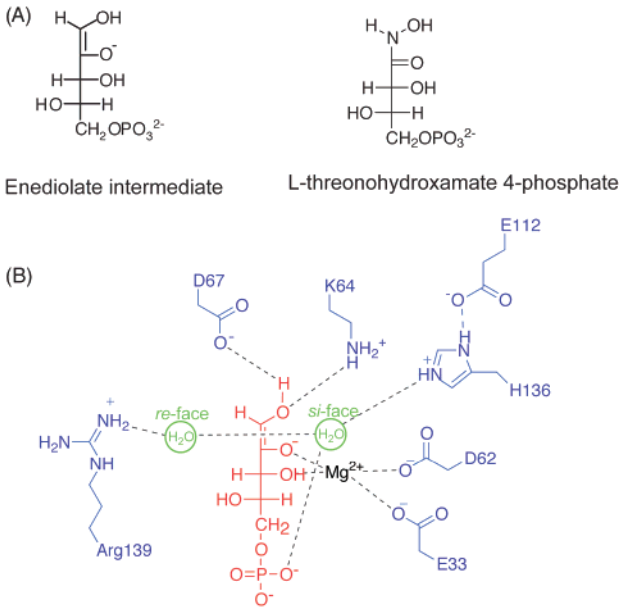

FIGURE 2: (A) Chemical structures of the L-threonohydroxamate 4-phosphate intermediate analogue and the enediolate intermediate of the KGPDC reaction. (B) Schematic representation of the binding of the enediolate intermediate in the KGPDC active site. Two ordered water molecules, marked with green circles, were observed in the active site. These water molecules are positioned on the *re*- and *si*-faces of N1 of the intermediate analogue and are labeled accordingly. Hydrogen bonds between these water molecules and active site residues are represented with dashed lines.

Table 1: Data Collection Statistics

	KGPDC K64A·L-THP	KGPDC H136A·L-THP	KGPDC E112Q·L-THP	KGPDC E112Q/H136A·L-THP
wavelength (Å)	0.961	1.514	0.961	0.961
source	APS 19ID	Cu Kα	APS 19ID	APS 19ID
unit cell dimensions	$a = 123.2$ Å, $b = 42.1$ Å, $c = 91.1$ Å, $\beta = 97.1°$	$a = 123.2$ Å, $b = 42.1$ Å, $c = 91.1$ Å, $\beta = 97.1°$	$a = 122.8$ Å, $b = 41.9$ Å, $c = 91.0$ Å, $\beta = 97.2°$	$a = 122.8$ Å, $b = 41.8$ Å, $c = 90.9$ Å, $\beta = 97.2°$
resolution (Å)[a]	1.7 (1.86−1.77)	1.9 (1.96−1.90)	1.8 (1.86−1.80)	1.9 (1.97−1.90)
no. of unique reflections	64983	37040	42753	36432
no. of total reflections	510441	902363	415129	571220
completeness (%)	99.5 (99.6)	99.2 (91.8)	95.1 (96.2)	98.2(98.1)
average I/σ[a]	25.6 (5.35)	26.0 (3.1)	14.0 (3.2)	18.1 (2.62)
R_{merge}[a,b]	0.063 (0.234)	0.065 (0.373)	0.066 (0.240)	0.081 (0.292)

[a] The values in parentheses give the statistics for the highest-resolution shell. [b] $R_{merge} = (\sum|I_{hkl} - I|/\sum I_{hkl}) \times 100$, where the average intensity I is taken over all symmetry equivalent measurements and I_{hkl} is the measured intensity for a given reflection.

KGPDC catalyzes exchange of the 1-*pro-S* proton of the L-xylulose 5-phosphate product with solvent, the H136A mutant cannot.

Additional biochemical evidence, however, suggests that His136 does not act alone in the mechanism of proton delivery. First, the incorporation of a solvent-derived proton in the enzyme-catalyzed reaction occurs at the 1-*pro-R* position as well as the 1-*pro-S* position of the reaction product, L-xylulose 5-phosphate. Incorporation at the 1-*pro-S* position (resulting in inversion of configuration) is favored over the 1-*pro-R* position (retention of configuration) in a roughly 2:1 ratio. Second, while the H136A mutant is unable to catalyze exchange of either proton on C1 with the solvent, it readily catalyzes the decarboxylation of 3-keto-L-gulonate 6-phosphate into L-xylulose 5-phosphate, but does so with a complete loss of stereoselectivity (*11*). These findings suggest that His136 does not function alone as the general acid for protonation of the intermediate. Several other potential catalytic acids, including Lys64, Glu112, Arg139, and two ordered water molecules, are located in the active site and are thus candidates for this function.

Interestingly, substitutions of Lys64 and Glu112 do not significantly reduce the activity for the decarboxylase reaction but rather affect the stereochemical course of the reaction (*11*). In the case of either the E112Q or K64A single mutant, decarboxylation occurs in a stereospecific manner with proton incorporation occurring exclusively at the 1-*pro-S* position. This change is somewhat surprising because Glu112 does not interact directly with the analogue of the enediolate intermediate, while Lys64 forms hydrogen bonds with the oxygen atoms of the enediolate. Perhaps even more surprising is the fact that the reaction catalyzed by the E112Q/H136A double mutant is also stereospecific but proton incorporation occurs at the 1-*pro-R* position instead, opposite that of the E112Q and K64A mutants. The R139V mutant also incorporates a proton exclusively at the 1-*pro-S* position, although the reason for the change is even less clear since this residue does not interact directly with either the substrate or the intermediate.

The lack of specificity of the protonation step in the wild-type reaction and the alterations in the stereochemical fate of the enediolate anion caused by mutation of active site residues can be explained in two ways. First, the active site contains multiple general acids, or second, the enediolate anion exists as a mixture of both the *cis* and *trans* configurations. The currently available biochemical evidence does not distinguish between these possibilities, although L-THP binds exclusively in a *cis* arrangement in the active site of wild-type KGPDC. To address these questions, the X-ray structures of K64A, H136A, E112Q, and E112Q/H136A mutants, each with L-THP bound in the active site, have been determined to 1.7, 1.9, 1.8, and 1.9 Å resolution, respectively. These structures provide strong evidence that the changes in the stereochemical course result from changes in the positions of two water molecules relative to the *cis*-enediolate intermediate. These water molecules evidently take part in two competing proton relay systems that deliver protons to the intermediate in a manner distinct from that of proton delivery in the OMPDC-catalyzed reaction, which further underscores the mechanistic differences within the OMPDC suprafamily.

MATERIALS AND METHODS

Creation of KGPDC Mutants. Site-directed mutants of KGPDC were introduced into the *UlaD* gene, which encodes KGPDC, using the QuikChange kit (Stratagene) (*11*). The DNA sequences of each mutant were verified, and the protein was expressed in the BLR(DE3) *recA*$^-$ strain of *E. coli* and purified as previously described for wild-type KGPDC (*4*).

Crystallization of KGPDC Mutants. Purified KGPDC was dialyzed against 50 mM HEPES (pH 7.5), 5 mM $MgCl_2$, and 100 mM NaCl, concentrated to 15 mg/mL, flash-frozen in liquid nitrogen, and stored at −80 °C. Crystals of KGPDC were grown by a microbatch method (*12*) by combining 10 μL of protein solution and 10 μL of a solution containing 16% MePEG 5000, 100 mM BTP (pH 7.0), 5 mM $MgCl_2$, and 25 mM L-threonohydroxamate 4-phosphate as described previously (*3*). All four of the KGPDC mutants crystallized in space group *C*2 with two KGPDC molecules in the asymmetric unit. Cell dimensions for each complex after freezing are given in Table 1.

Synthesis of L-Threonohydroxamate 4-Phosphate. L-Threonohydroxamate was prepared from calcium threonate and purified by anion exchange chromatography as described previously (*10*).

Crystal Freezing and Data Collection. Crystals of the mutant variants of KGPDC grown in the presence of 25 mM L-threonohydroxamate 4-phosphate were transferred in two steps for approximately 30 s to a cryoprotecting solution containing 15% MePEG 5000, 100 mM PIPES (pH 7.0), 15% ethylene glycol, 200 mM NaCl, and 50 mM L-

Table 2: Refinement Statistics

	KGPDC K64A·L-THP	KGPDC H136A·L-THP	KGPDC E112Q·L-THP	KGPDC E112Q/H136A·L-THP
resolution limits (Å)	91−1.7	91−1.9	91−1.8	91−1.9
R_{factor} (%)	16.2	14.8	15.6	15.8
R_{free} (%)	20.5	19.2	19.6	20.8
no. of reflections (working set)	58994	34888	39925	32895
no. of reflections (test set)	3135	1839	2116	1736
no. of protein atoms	3274	3298	3269	3267
no. of solvent atoms	593	532	413	468
average *B* factor (Å^2)	17.0	20.0	15.6	15.4
rmsd for bond lengths (Å)	0.017	0.015	0.013	0.016
rmsd for bond angles (deg)	1.61	1.53	1.38	1.51

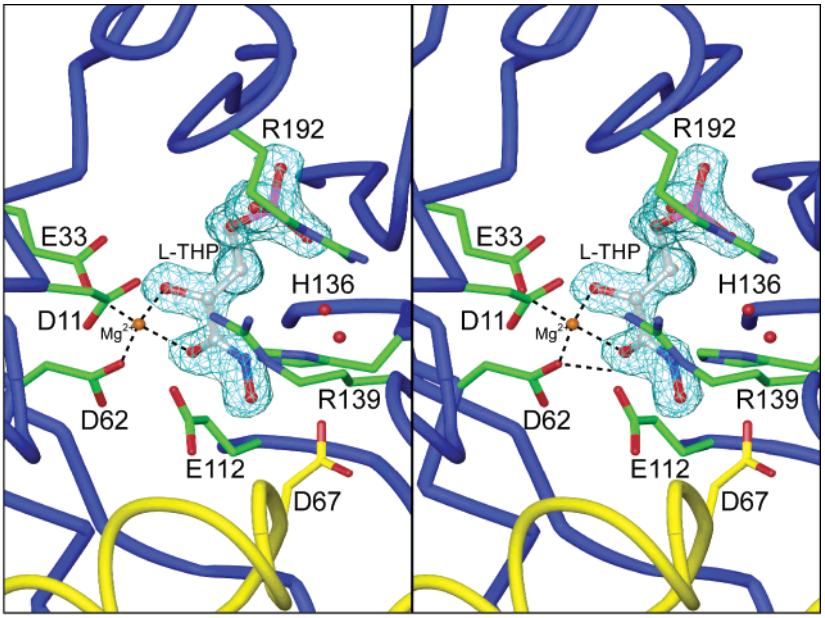

FIGURE 3: Sample electron density for the L-threonohydroxamate 4-phosphate intermediate analogue used in these studies. Shown is the electron density for the K64A mutant.

threonohydroxamate 4-phosphate. The crystals were flash-frozen in a cold nitrogen stream at −160 °C prior to data collection.

Data for the K64A, E112Q, and E112Q/H136A mutants were collected to 1.7, 1.8, and 1.9 Å resolution, respectively, at beamline 19ID of the Structural Biology Center at the Advanced Photon Source (Argonne National Laboratory, Argonne, IL) with a single 180° scan with 1° oscillations for a duration of 2 s per frame. The data were integrated and scaled with HKL2000 (*13*). Data for the H136A mutant were collected to 1.9 Å resolution in a single 180° scan with 0.5° oscillations for a duration of 5 min per frame with an RAxisIV image plate detector using copper Kα radiation from a Rigaku rotating anode generator. The data were scaled and integrated utilizing HKL2000 (*13*). Data collection statistics are listed in Table 1.

Structure Determination and Refinement. The structures of each KGPDC mutant were determined by molecular replacement with Molrep (*14*, *15*) starting from the previously published structure of KGPDC·L-gulonate 6-phosphate (*3*). Each model was improved by refinement with Refmac (*14*, *16*, *17*). Solvent atoms were added to each model using ARPwARP (*18*). The final values for R_{factor} and R_{free} for each refined structure are listed in Table 1.

A Ramachandran plot indicates that 95% of the residues in the K64A structure fall in the most favorable regions with the remaining 5% falling in the additionally allowed regions as determined with Procheck (*19*). For the E112Q structure, 95.0% of the residues fall in the most favorable regions with the remaining 5.0% falling in the additionally allowed regions, and for the E112Q/H136A structure, 94.8% of the residues fall in the most favorable regions with the remaining 5.2% falling in the additionally allowed regions. Sample electron density for the K64A mutant is shown in Figure 3.

RESULTS

Like wild-type KGPDC, each mutant crystallized with a dimer of identical $(\beta/\alpha)_8$-barrel subunits in the crystallographic asymmetric unit. In each structure, the electron density for both subunits in the dimer was continuous and well-defined for the entire length of the polypeptide from Ala2 to Trp215. Likewise, the electron density for L-THP was unambiguous for all complexes, and the planar nature of the hydroxamate group was clearly evident. Importantly, in all four structures, the *cis* geometry of hydroxamate group was unequivocal; that is to say, the oxygen on the nitrogen atom was located on the same side of the C−N bond as the oxygen of the carbonyl group.

In each of the structures, the mutation of Lys64, Glu112, or His136 resulted in changes in the positions of two ordered water molecules relative to their positions in the wild-type structure. In the wild-type structure, one water molecule is positioned approximately 2 Å from the *si*-face of N1 of the

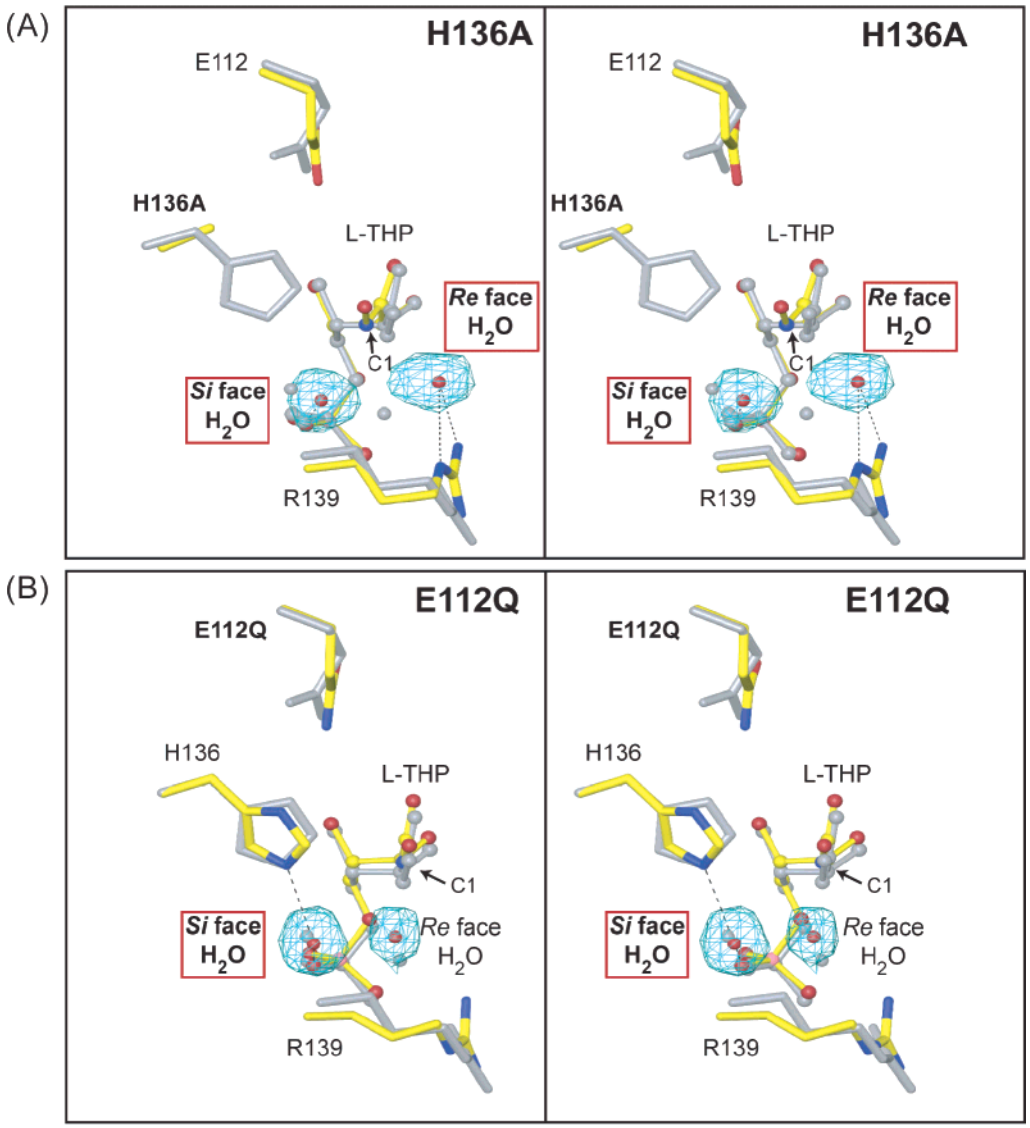

FIGURE 4: Stereoviews of the KGPDC active site for the H136A mutant (A) and the E112Q mutant (B). Red boxes denote the water molecules that are properly positioned to transfer a proton to the enediolate. In the H136A mutant, both the *si*-face and *re*-face water molecules, highlighted with red boxes, are capable of transferring a proton to C1 of the endiolate from either face. In the E112Q mutant, only the *si*-face water molecule, highlighted with a red box, is in a position to transfer a proton from C1 to the enediolate (*si*-face). These residue side chains and the two water molecules in the wild-type enzyme are shown in gray.

hydroxamate group and forms hydrogen bonds with both the His136 side chain and the phosphate group of L-THP (Figure 2B). The second water is observed near the *re*-face of N1 of the hydroxamate group and forms hydrogen bonds with the water molecule located on the *si*-face and with NH1 of Arg139. These two water molecules will be termed the *si*- and *re*-face waters. The changes in the positions of these water molecules, which are part of a complex hydrogen bond network in the active site, are central to understanding the alterations in the stereospecificity of the proteins induced by the mutations as described below.

Structure of KGPDC H136A·L-THP. The histidine to alanine substitution was clearly evident in the electron density for the H136A mutant. As a result of the mutation, the Glu112 side chain, which forms a hydrogen bond with the His136 side chain in the structure of wild-type KGPDC, undergoes a small rearrangement so that it turns away from the position of His136 in wild-type KGPDC. In addition, both the *re*-face water and the *si*-face waters move so that both are equidistant from the nitrogen atom of the hydroxamate (Figure 4A). The *re*-face water moves more than 2 Å so that it forms hydrogen bonds with both Nϵ and NH1 of Arg139, the side chain of which moves closer to the hydroxamate and undergoes a slight conformational change to accommodate the *re*-face water molecule. These changes in the positions of the water molecules likely result from a slight shift in the hydroxamate that allows N1, C1, and C2 to move toward the space previously occupied by His136 in the wild-type enzyme. In this arrangement, both water molecules are roughly 2.9 Å from C1 of the intermediate analogue and are positioned to transfer a proton to either face of the enediolate intermediate in the H136A mutant.

Structure of KGPDC E112Q·L-THP. While the change from glutamate to glutamine could not be detected from the electron density in the E112Q structure, the E112Q substitution causes the Gln side chain to rotate away from His136, which disrupts the hydrogen bond between His136 and Glu112 that was observed in the wild-type structure. Both the *re*-face water and the hydroxamate also move substantially from their positions in the structure of the wild-type

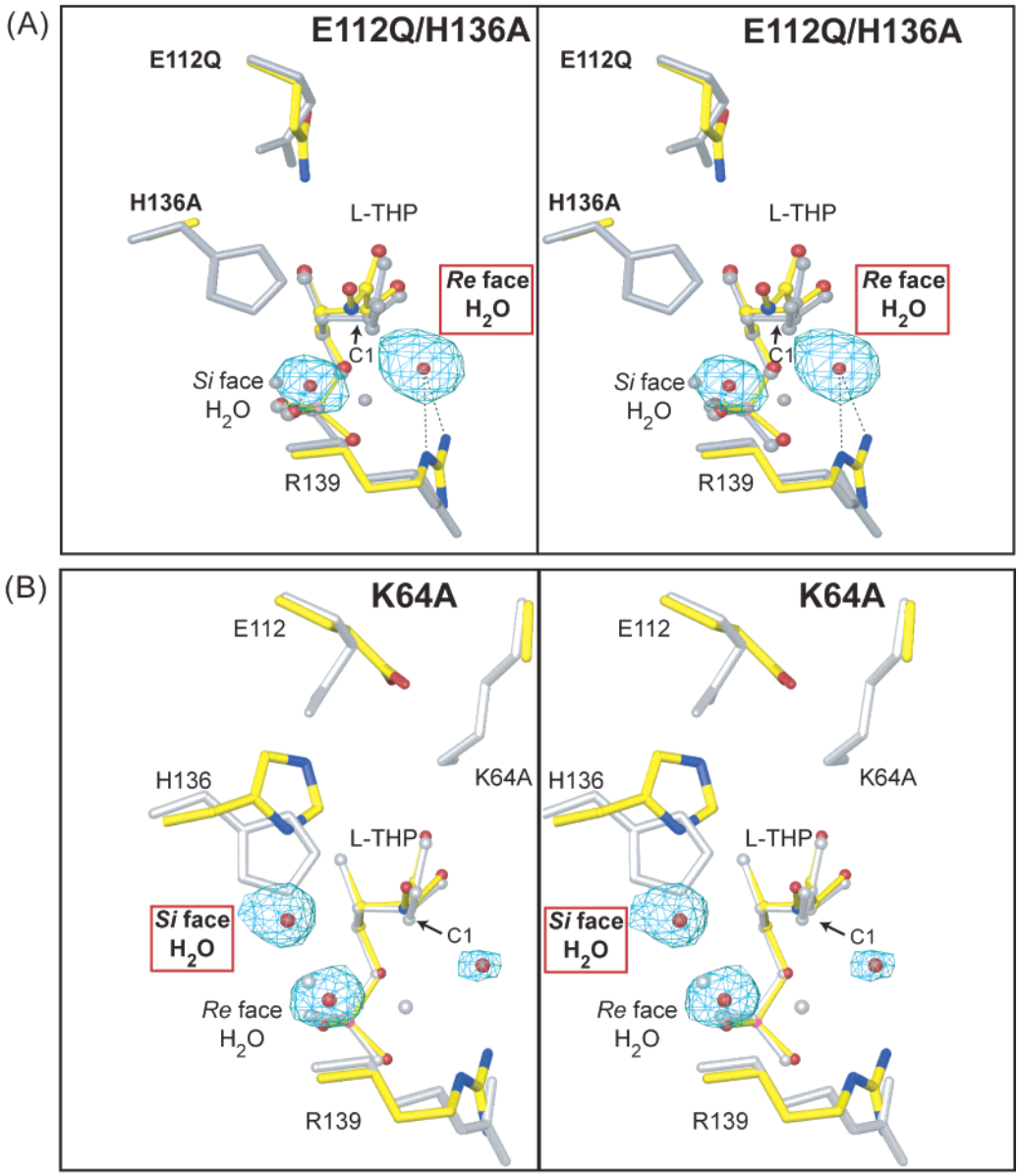

FIGURE 5: Stereoviews of the KGPDC active site for the H136A/E112Q mutant (A) and the K64A mutant (B). Red boxes denote the water molecules that are properly positioned to transfer a proton to the enediolate. In the E112Q/H136A mutant, only the *re*-face water molecule, highlighted with a red box, is capable of transferring a proton to C1 of the enediolate (*re*-face). In the K64A mutant, only the *si*-face water molecule, highlighted with a red box, is capable of transferring a proton to C1 of the enediolate (*si*-face). These residue side chains and the two water molecules in the wild-type enzyme are shown in gray.

enzyme (Figure 4B). The hydroxamate undergoes a slight conformational change that causes atoms N1, C1, and C2 to move toward the position of Gln112. The *re*-face water molecule moves 1.5 Å closer to O1 of the hydroxamate so that it is positioned in the plane of the N1−C1 bond of the hydroxamate. The position of the *si*-face water changes only slightly and remains in a position to transfer a proton to C1 of the intermediate even though the orientation of the side chain of His136 is perturbed by the mutation. The alteration of the orientation of His136 results from the disruption of the hydrogen bond between this residue and Glu112, which causes the imidazole ring of histidine to rotate about the bond between Cβ and Cγ so that it forms a hydrogen bond with the side chain of Thr114 instead of Glu112 (now a glutamine). As a result of these changes in the active site, only the *si*-face water molecule is appropriately positioned to transfer a proton to the enediolate intermediate in the E112Q mutant.

Structure of KGPDC E112Q/H136A·L-THP. The absence of the histidine side chain was clearly evident in the electron density for the structure of the E112Q/H136A double mutant. As in the E112Q mutant, the glutamate to glutamine substitution could not be discerned from the electron density but also results in a change in the hydrogen bond network that allows the side chain of Gln112 to turn away from the active site. These changes bring about substantial alterations in the positions of both the *re*- and *si*-face water molecules (Figure 5A). The *si*-face water moves 1.0 Å closer to the hydroxamate group so that it is in the plane of the N1−C1 bond of the hydroxamate. The *re*-face water molecule moves 2.4 Å and takes part in hydrogen bonding interactions with the side chain of Arg139, which as in the H136A mutant,

adopts a slightly different conformation to accommodate the *re*-face water molecule. The mutations also bring about changes in the position of the hydroxamate, which moves through rotations about the bonds linking N1, C1, and C2 of the molecule. This alteration in the position of the hydroxamate is greater in the double mutant than in any of the single mutants. The N1 atom, equivalent to C1 of the intermediate, moves 1.2 Å closer to the position formerly occupied by the side chains of His136 and Gln112.

Structure of KGPDC K64A·L-THP. The lysine to alanine substitution could easily be discerned in the electron density for the K64A mutant protein structure. Although Lys64 has been suggested to play a role in the stabilization of the *cis*-enediolate, the loss of interactions that resulted from the lysine to alanine substitution did not cause any changes in the conformation of L-THP. This substitution did, however, bring about substantial changes in the positions of the Glu112 and H136 side chains as well as the *re*- and *si*-face water molecules. These changes are similar to those seen in the E112Q structure, although the movements of the side chains for Glu112 and His136 and both water molecules are more pronounced in this mutant (Figure 5B). This substitution causes the side chain of His136 to move away from the enediolate and toward the space formerly occupied by the lysine side chain. As a result, both the *re*- and *si*-face water molecules are observed on the *si*-face of C1 of the enediolate. A third water molecule is observed near the side chain of Arg139, which also undergoes a small conformational change.

DISCUSSION

The unusual changes in the stereochemical course of the decarboxylation reaction catalyzed by the four KGPDC mutants studied here cannot be explained easily by either existing biochemical data or existing structures of the wild-type enzyme (*3*, *10*, *11*). While there is ample evidence that both His136 and Glu112 are involved in the mechanism of transfer of a proton to the enediolate, in the absence of structural data, their individual roles were not clear, nor was it clear why changes in these two residues can alter the stereochemistry of the reaction to such an extent. The H136A substitution results in a complete loss of stereoselectivity for the reaction but, when combined with the E112Q substitution, causes the enzyme to catalyze stereospecific incorporation of only the 1-*pro*-*R* proton. The E112Q substitution alone, however, causes the enzyme to catalyze stereospecific incorporation of the opposite proton on C1.

One possible explanation for the lack of stereospecificity in the decarboxylation reaction catalyzed by wild-type KGPDC is that it may be possible for the enediolate to adopt either a *cis* or *trans* configuration in the active site. This would require that carbon dioxide, which leaves in the first step of the KGPDC reaction, depart from either side of the bond between C2 and C3 of the substrate to generate the enediolate intermediate as a mixture of both *cis* and *trans* configurations. Once the enediolate is formed, interactions between the C1 and C2 oxygen atoms and the side chains of Lys64 and Asp67 presumably form a high energetic barrier that would prevent the interconversion of *cis* and *trans* enediolate intermediates. The addition of a proton from a single catalytic acid would then result in nonstereospecific proton incorporation at either position of the hydroxymethylene group of L-xylulose 5-phosphate. A possible explanation for the increase in the extent of incorporation at the 1-*pro*-*R* position in the H136A and H136A/E112Q mutants might be that, in these mutants, a *trans*-enediolate is preferentially formed. The structures of both the H136A and E112Q/H136A mutants, however, provide no evidence of the existence of a *trans*-enediolate. In both structures, it is clear from the electron density that the enediolate analogue is bound exclusively in a *cis* configuration. In addition, no major changes are observed in the locations of the Lys64 and Asp67 side chains, both of which stabilize the *cis*-enediolate and would have to be positioned differently to accommodate a *trans*-enediolate. Furthermore, even in the K64A mutant, there is no change in the configuration of the enediolate as might be expected since this residue appears to be important for stabilizing the enediolate.

Instead, the structural evidence supports a mechanism for the protonation of the intermediate that involves two acids in the active site that protonate a *cis*-enediolate intermediate from opposite sides. While the His136 side chain may be positioned to deliver a proton to the *si*-face of C1 of the enediolate for incorporation at the *pro*-*S* position, there is no corresponding amino acid side chain on the *re*-face of C1 to deliver a proton for incorporation at the *pro*-*R* position. Furthermore, the mutations studied here do not introduce any detectable changes in the positions of any active site residues that would allow them to act as a *re*-face acid. Although small changes were observed in the orientation and position of several side chains, including, most notably that of Glu112, they did not move any residue closer to either face of the enediolate intermediate. In fact, Glu112 moves away from the enediolate, which makes it less likely that it transfers a proton directly to the enediolate.

The most obvious mechanism for delivery of a proton to the enediolate intermediate involves the *re*- and *si*-face water molecules. Given that the pK_a of the hydroxymethylene group of the L-xylulose 5-phosphate product is likely 20−22, the pK_a difference between the *cis*-enediolate intermediate and these water molecules is sufficiently large to allow either of these water molecules to act as general acids and to competitively protonate the intermediate from either side. In the structure of the wild-type enzyme, both molecules are positioned on either face of the enediolate to transfer a proton to the enediolate, although the *re*-face water molecule is positioned slightly more toward N1 of the hydroxamate. A possible reason for this may be that a hydrogen bond, formed between this water molecule and N1 of the intermediate analogue, may be altering the position of this water molecule slightly as compared to its position in the presence of the actual enediolate. In the structures of the K64A, E112Q, and E112Q/H136A mutants, changes in the positions of these water molecules relative to the enediolate analogue correlate with the observed stereochemistry for the decarboxylation reaction (*11*). In the structures of the K64A and E112Q mutants, only the *si*-face water is positioned to transfer a proton to the enediolate, consistent with biochemical experiments that demonstrated that proton incorporation occurs exclusively at the *pro*-*S* position of L-xylulose 5-phosphate. In the structure of the E112Q/H136A mutant, only the *re*-face water is positioned to transfer a proton to the enediolate, consistent with biochemical experiments that showed that

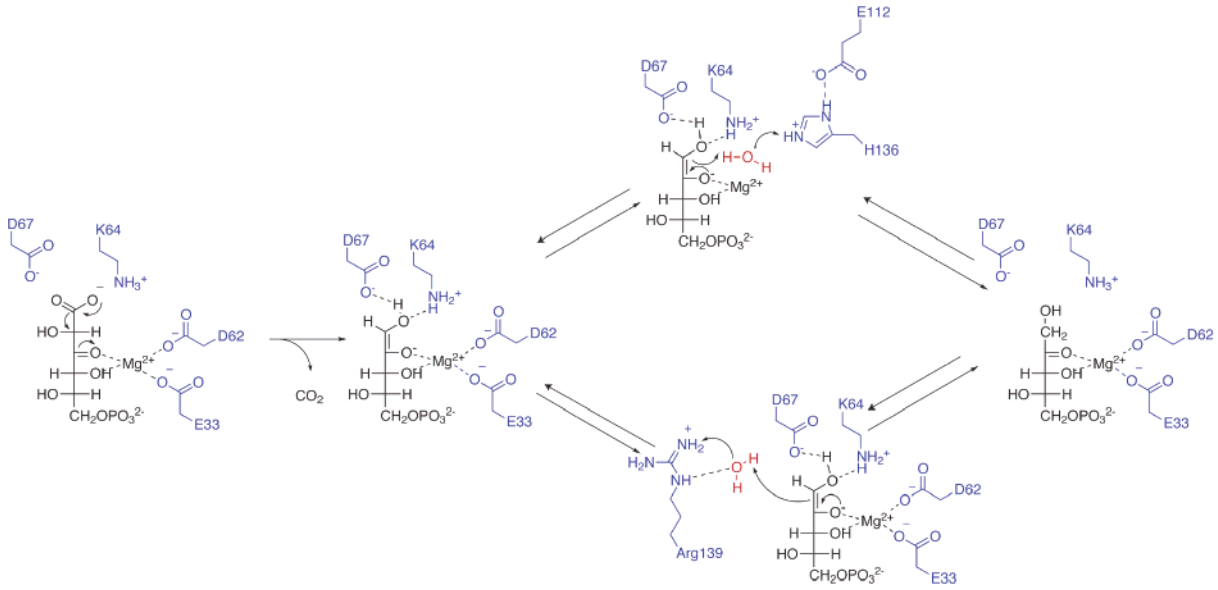

FIGURE 6: Proposed mechanism for the KGPDC reaction. The loss of carbon dioxide results in the formation of a Mg^{2+} ion-stabilized enediolate. The addition of a proton to either face of the enediolate intermediate results in proton incorporation at both the *pro-R* and *pro-S* positions. Two water molecules in the active site may alternately function as proton shuttles to transfer a proton from the His136 side chain or the Arg139 side chain to either face of the enediolate to generate the reaction product, L-xylulose 5-phosphate.

the 1-*pro-R* position of L-xylulose 5-phosphate was protonated. In the structure of the H136A mutant, both water molecules are positioned to transfer a proton to the enediolate, consistent with stereorandom incorporation of a proton in this mutant.

Interactions between these two water molecules and protonated active site residues likely act to position these water molecules correctly for proton delivery. Given the high pK_a of the hydroxymethylene group of the L-xylulose 5-phosphate, enhancement of the acidity of the water molecules by interactions with other polar group is probably unnecessary, but may provide a route for proton transfer. In the wild-type enzyme, the *si*-face water forms a hydrogen bond with the His136 side chain, which likely is sufficiently acidic to protonate the water molecule so that it may act as a proton shuttle to protonate the enediolate. The hydrogen bond between His136 and Glu112 may act to correctly position the imidazole ring nitrogen relative to the enediolate. The His136 side chain itself may also act directly to transfer a proton directly to the enediolate intermediate rather than doing so via the *si*-face water molecule. Although it is difficult to distinguish between these two possibilities, the *si*-face water molecule is better positioned to transfer a proton to the enediolate and would seem to be the most likely candidate for this role.

The *re*-face water molecule participates in similar interactions with the side chain of Arg139 in the H136A and E112Q/H136A structures. This interaction presumably orients this water sufficiently so that it can transfer a proton to the *re*-face of the enediolate. Thus, the *re*-face water molecule serves as a proton shuttle to transfer a proton from Arg139 to the enediolate. Because Arg139 is exposed to the solvent, proton exchange between it and the solvent may occur rapidly. The large distance between the Arg139 side chain and the enediolate makes it unlikely that Arg139 acts directly as a general acid. In addition, stacking interactions between the side chains of Arg139 and Arg192 likely limit the movement of Arg139 so that it cannot move closer to the enediolate. This role for Arg139 is consistent with the biochemical studies of the R139V mutant, which catalyzes proton incorporation exclusively in the 1-*pro-S* position.

From these structures, a clearer picture of the mechanism of KGPDC can be drawn (Figure 6). Previous structural and biochemical studies have demonstrated that the KGPDC reaction proceeds through an enediolate intermediate that is stabilized through interactions with the required Mg^{2+} ion and the side chains of the conserved Lys64 and Asp67 residues. The observation that L-THP is bound in a *cis* geometry in the wild-type enzyme and all four of the mutants described here provides further evidence that the enediolate forms exclusively in a *cis* geometry following the departure of carbon dioxide, as had been previously suggested (*10*). The side chains of Lys64 and Asp67 act not only to stabilize this intermediate but also to enforce the *cis* geometry so that the enediolate is properly positioned for the addition of a proton to either face.

Through a proton relay system involving two water molecules in the active site, the side chains of His136 and Arg139 function as the ultimate proton sources in the KGPDC reaction to competitively deliver a proton to the C1 position of the enediolate intermediate. Whether proton incorporation occurs at the *pro-S* position or the *pro-R* position depends on which of these two residues acts as the ultimate source for the proton. Similar proton relay systems have been proposed for pyruvate kinase and deoxyribose-5-phosphate aldolase (*20*, *21*). On the basis of crystal structures of both of these enzymes, ordered water molecules were proposed to function as proton shuttles to deliver a proton to a reaction intermediate.

CONCLUSIONS

The elucidation of the proton delivery mechanism in the KGPDC-catalyzed reaction further underscores the mechanistic differences between KGPDC and OMPDC. Although they are homologous enzymes and share a conserved active site architecture, the mechanisms of the reactions they

catalyze are completely different. These studies further demonstrate the wide disparity in the use of this active site architecture by each enzyme. In particular, the mechanism of proton delivery in each enzyme is completely unrelated. In OMPDC, the conserved lysine residue homologous to Lys64 in KGPDC acts as the proton donor. The structures described here, along with previous biochemical analysis, demonstrate that the mechanism of proton delivery in KGPDC is completely unrelated to that of OMPDC and involves water molecules that shuttle protons from His136 and Arg139 to the *cis*-enediolate intermediate. Interestingly, neither of these residues is conserved with OMPDC. Although it plays no role in general acid catalysis in KGPDC, the conserved Lys64 plays an equally important role in the KGPDC-catalyzed reaction where it serves to stabilize and position the *cis*-enediolate intermediate. These studies further define the catalytic roles of conserved residues in the active site of KGPDC and demonstrate that even though KGPDC and OMPDC share a common active site architecture, each enzyme uses this architecture to catalyze reactions with unrelated substrate specificity and unrelated reaction mechanisms.

REFERENCES

1. Hocker, B., Beismann-Driemeyer, S., Hettwer, S., Lustig, A., and Sterner, R. (2001) Dissection of a $(\beta/\alpha)_8$-barrel enzyme into two folded halves, *Nat. Struct. Biol. 8*, 32−36.
2. Gerlt, J. A., and Babbitt, P. C. (1998) Mechanistically diverse enzyme superfamilies: the importance of chemistry in the evolution of catalysis, *Curr. Opin. Chem. Biol. 2*, 607−612.
3. Wise, E., Yew, W. S., Babbitt, P. C., Gerlt, J. A., and Rayment, I. (2002) Homologous $(\beta/\alpha)_8$-barrel enzymes that catalyze unrelated reactions: orotidine 5′-monophosphate decarboxylase and 3-keto-L-gulonate 6-phosphate decarboxylase, *Biochemistry 41*, 3861−3869.
4. Yew, W. S., and Gerlt, J. A. (2002) Utilization of L-ascorbate by *Escherichia coli* K-12: assignments of functions to products of the yjf-sga and yia-sgb operons, *J. Bacteriol. 184*, 302−306.
5. Miller, B. G., and Wolfenden, R. (2002) Catalytic proficiency: the unusual case of OMP decarboxylase, *Annu. Rev. Biochem. 71*, 847−885.
6. Harris, P., Navarro Poulsen, J. C., Jensen, K. F., and Larsen, S. (2000) Structural basis for the catalytic mechanism of a proficient enzyme: orotidine 5′-monophosphate decarboxylase, *Biochemistry 39*, 4217−4224.
7. Miller, B. G., Hassell, A. M., Wolfenden, R., Milburn, M. V., and Short, S. A. (2000) Anatomy of a proficient enzyme: the structure of orotidine 5′-monophosphate decarboxylase in the presence and absence of a potential transition state analog, *Proc. Natl. Acad. Sci. U.S.A. 97*, 2011−2016.
8. Wu, N., Mo, Y., Gao, J., and Pai, E. F. (2000) Electrostatic stress in catalysis: structure and mechanism of the enzyme orotidine monophosphate decarboxylase, *Proc. Natl. Acad. Sci. U.S.A. 97*, 2017−2022.
9. Appleby, T. C., Kinsland, C., Begley, T. P., and Ealick, S. E. (2000) The crystal structure and mechanism of orotidine 5′-monophosphate decarboxylase, *Proc. Natl. Acad. Sci. U.S.A. 97*, 2005−2010.
10. Wise, E. L., Yew, W. S., Gerlt, J. A., and Rayment, I. (2003) Structural evidence for a 1,2-enediolate intermediate in the reaction catalyzed by 3-keto-L-gulonate 6-phosphate decarboxylase, a member of the orotidine 5′-monophosphate decarboxylase suprafamily, *Biochemistry 42*, 12133−12142.
11. Yew, W. S., Wise, E. L., Rayment, I., and Gerlt, J. A. (2004) Evolution of Enzymatic Activities in the Orotidine 5′-Monophosphate Decarboxylase Suprafamily: Mechanistic Studies of the Reaction Catalyzed by 3-Keto-L-Gulonate 6-Phosphate Decarboxylase, *Biochemistry 43*, 6427−6437.
12. Rayment, I. (2002) Small-scale batch crystallization of proteins revisited. An underutilized way to grow large protein crystals, *Structure 10*, 147−151.
13. Otwinowski, Z., and Minor, W. (1997) Processing of X-ray diffraction data collected in oscillation mode, *Methods Enzymol. 276*, 307−326.
14. Collaborative Computational Project No. 4 (1994) The CCP4 Suite: Programs for protein crystallography, *Acta Crystallogr. D50*, 760−763.
15. Vagin, A., and Teplyakov, A. (2000) An approach to multi-copy search in molecular replacement, *Acta Crystallogr. D56*, 1622−1624.
16. Roussel, A., and Cambillau, C. (1991) Turbo Frodo, in *Silicon Graphics Geometry Partners Directory*, Silicon Graphics, Mountain View, CA.
17. Murshudov, G. N., Vagin, A. A., and Dodson, E. J. (1997) Refinement of Macromolecular Structures by the Maximum-Likelihood Method, *Acta Crystallogr. D53*, 240−255.
18. Perrakis, A., Morris, R., and Lamzin, V. S. (1999) Automated protein model building combined with iterative structure refinement, *Nat. Struct. Biol. 6*, 458−463.
19. Laskowski, R. A., MacArthur, M. W., Moss, D. S., and Thornton, J. M. (1993) PROCHECK: a program to check the stereochemical quality of protein structures, *J. Appl. Crystallogr. 26*, 283−291.
20. Heine, A., DeSantis, G., Luz, J. G., Mitchell, M., Wong, C. H., and Wilson, I. A. (2001) Observation of covalent intermediates in an enzyme mechanism at atomic resolution, *Science 294*, 369−374.
21. Larsen, T. M., Benning, M. M., Rayment, I., and Reed, G. H. (1998) Structure of the bis(Mg^{2+})-ATP-oxalate complex of the rabbit muscle pyruvate kinase at 2.1 Å resolution: ATP binding over a barrel, *Biochemistry 37*, 6247−6255.
22. Carson, M. (1997) Ribbons, *Methods Enzymol. 277*, 493−505.

BI0497392